

*Reprinted from*

JOURNAL  
OF THE  
PHYSICAL  
SOCIETY  
OF  
JAPAN



■ FULL PAPER

**Charge Neutral Fermionic States and Current Oscillation  
in a Graphene–Superconductor Hybrid Structure**

Wenye Duan, Wei Wang, Chao Zhang, Kuijuan Jin, and Zhongshui Ma

J. Phys. Soc. Jpn. **85**, 104713 (2016)

## Charge Neutral Fermionic States and Current Oscillation in a Graphene–Superconductor Hybrid Structure

Wenye Duan<sup>1</sup>, Wei Wang<sup>1</sup>, Chao Zhang<sup>2</sup>, Kuijuan Jin<sup>3,4</sup>, and Zhongshui Ma<sup>3,4</sup>

<sup>1</sup>*School of Physics, Peking University, Beijing 100871, China*

<sup>2</sup>*School of Physics, University of Wollongong, New South Wales 2522, Australia*

<sup>3</sup>*Beijing National Laboratory for Condensed Matter Physics, Institute of Physics, Chinese Academy of Sciences, Beijing 100190, China*

<sup>4</sup>*Collaborative Innovation Center of Quantum Matter, Beijing 100871, China*

(Received May 26, 2016; accepted August 31, 2016; published online September 27, 2016)

The proximity properties of edge currents in the vicinity of the interface between the graphene and superconductor in the presence of magnetic field are investigated. It is shown that the edge states introduced by Andreev reflection at the graphene–superconductor (G/S) interface give rise to the charge neutral states in all Landau levels. We note that in a topological insulator–superconductor (TI/S) hybrid structure, only  $N = 0$  Landau level can support this type of charge neutral states. The different interface states of a G/S hybrid and a TI/S hybrid is due to that graphene consists of two distinct sublattices. The armchair edge consists of two inequivalent atoms. This gives rise to unique electronic properties of edge states when connected to a superconductor. A direct consequence of zero charge states in all Landau levels is that the current density approaches zero at interface. The proximity effect leads to quantum magnetic oscillation of the current density in the superconductor region. The interface current density can also be tuned with a finite interface potential. For sharp  $\delta$ -type interface potential, the derivative of the wavefunction is discontinuous. As a result, we found that there is current density discontinuity at the interface. The step of the current discontinuity is proportional to the strength of the interface potential.

### 1. Introduction

A graphene–superconductor (G/S) hybrid structure can exhibit interesting physics not seen in any other systems, e.g., the specular Andreev reflection (SAR).<sup>1,2</sup> Prior to the discovery of graphene, only the Andreev retro-reflection can occur in a normal metal–superconductor (N/S) interface.<sup>3,4</sup> SAR provides a basis to experimental investigations of the proximity effect and supercurrent flow in G/S system. So far, most theoretical analysis on the G/S hybrid structure are carried out in absence of a magnetic field.<sup>5–8</sup> The edge states and distribution of edge currents in semi-infinite graphene under strong magnetic field provide a direct evidence of the connection between the edge states and topological properties of relativistic fermions.<sup>9</sup> Under a magnetic field smaller than the critical field of superconductor, but still large enough, the energy levels of the bulk states are quantized<sup>10,11</sup> and the edge states sprawl out at the interface. Under the magnetic field  $B$ , the unusual Landau levels (LLs) of graphene have a square-root dependence on both magnetic field and level index  $E_N = \text{sgn}(N)\sqrt{2e\hbar v_F^2|N|B}$ , where  $N$  is any integer.<sup>12</sup> Generally, the strong magnetic field makes the energy spacing between adjacent LLs larger than (or of the same order of) the typical superconducting pair potential ( $\Delta_0 \lesssim 1$  meV). As a consequence, the magnetic field is expected to affect the Andreev reflection (AR) in G/S junction. Akhmerov and Beenakker propose a method to detect the valley polarization of quantum Hall edge states, using a superconducting contact as a probe.<sup>13,14</sup> In their work the edges are assumed to be smooth on the scale of a magnetic length,  $l_B = \sqrt{\hbar/|eB|}$ , so that they may be treated locally as a straight line with a homogeneous boundary condition. For a G/S junction under a strong magnetic field, edge states are formed due to the confinement introduced by both the external magnetic field and the superconducting pair potential. These edge states

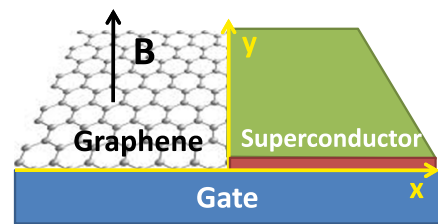


**Fig. 1.** (Color online) Schematic experimental setup with an armchair boundary.

produce the Hall current in the direction parallel to the interface. Physically, these edge states are a coherent superposition of electron and hole-like edge excitations similar to those realized in finite pn-junction quantum-Hall samples.<sup>14,15</sup>

In this paper, we will demonstrate that the interplay of the AR and skipping cyclotron orbits at the G/S interface gives rise to the charge neutral quasiparticles. Such a charge neutral state in a topological insulator–superconductor (TI/S) hybrid is a topic of intensive current research. Probing zero-modes using charge transport<sup>16</sup> and using quantum Hall edge states<sup>17</sup> have been established. Recently chiral edge states with neutral fermions has been observed in synthetic Hall ribbons.<sup>18</sup> We show a theoretical evidence that the charge neutral states do exist. Furthermore, in a TI/S hybrid, the charge neutral quasiparticles only exist in the  $N = 0$  Landau level.<sup>19</sup> In the present G/S hybrid structure, the charge neutral quasiparticles can also exist in the high LLs, which significantly enhances the probability of experimentally observing the states. Our analysis is based on a hybrid where graphene has an armchair edge at the boundary, as shown in Fig. 1. The hybrid with a zigzag boundary can be analyzed with the same method upon a suitable transformation.

The paper is organized as follows. In Sect. 2, we discuss the Hamiltonian and formulate the boundary conditions for the G/S hybrid. In Sect. 3 we analyse the wave-number-dependent excitation spectra and the effective charges of Landau levels. Section 4 is devoted to the analysis of edge current and Sect. 5 is a brief summary.

## 2. Hamiltonian and Boundary Conditions

The G/S hybrid with a contact in an armchair configuration is illustrated in Fig. 1, where a uniform magnetic field is applied in the direction perpendicular to the plane. We consider a type-I superconductor in our study so that the magnetic field is absent in the superconductor due to the Meissner effect. For simplicity, we also neglect the effect of magnetic penetration to the superconductor and the inhomogeneity of the magnetic field in the vicinity of the interface. The magnetic field is, then, expressed approximately in form of  $B(x) = B\Theta(-x)$ , where  $\Theta(x)$  is the Heaviside's step function.

For honeycomb hexagon lattice with two valley degrees of freedom ( $K$  and  $K'$ ) in the reciprocal space, the Hamiltonian of the system is given as

$$\hat{\mathcal{H}} = \begin{pmatrix} \hat{h} - E_F & \Delta \cdot I_4 \\ \Delta^* \cdot I_4 & E_F - T\hat{h}T^{-1} \end{pmatrix}, \quad (1)$$

and the states are described by Dirac–Bogoliubov–de Gennes (DBdG) equation<sup>1,20</sup>

$$\hat{\mathcal{H}}\Psi = E\Psi, \quad (2)$$

where

$$\hat{h} = \begin{pmatrix} \hat{h}_K & 0 \\ 0 & \hat{h}_{K'} \end{pmatrix} + U(x) + \hat{V}(x) \quad (3)$$

is the Dirac Hamiltonian in a form of  $4 \times 4$  matrix acting on two inequivalent sublattices and two valley degrees of freedom  $K$  and  $K'$ , respectively;  $I_4$  is a four-dimensional identity matrix;  $\Delta$  is the superconductor pair potential  $\Delta(\mathbf{r}) = \Delta_0 e^{i\phi} \Theta(x)$  with  $\Delta_0$  the excitation gap and  $\phi$  is the phase of

$\Delta(\mathbf{r})$  in the superconductor;  $T$  is the time-reversal operator;  $U$  is the potential  $U(x) = U_G\Theta(-x) + U_S\Theta(x)$  which is used to control the difference of Fermi energies in the two regions;  $\hat{V}(x) = \hat{V}\delta(x)$  is a  $4 \times 4$  matrix for the interface potential which describes the barrier effect of an interval insulator layer between the graphene and superconductor.

The two inequivalent Dirac cones are given as  $\mathbf{K} = (4\pi/(3\sqrt{3}a), 0)$  and  $\mathbf{K}' = (-4\pi/(3\sqrt{3}a), 0)$ , where  $a$  is the distance between neighbouring carbon atoms. For the contact of G/S in the armchair configuration, both inequivalent sublattices are on the interface. The wavefunction of DBdG equation can be written in the form

$$\Psi_A = e^{iKR_A}\psi_{AK} + e^{iK'R_A}\psi_{AK'}, \quad (4)$$

$$\Psi_B = e^{iKR_B}\psi_{BK} + e^{iK'R_B}\psi_{BK'}, \quad (5)$$

where  $\psi_{(A/B)(K/K')}$  are the components of the spinor  $\psi = (u, v)^T$ , in which  $u$  and  $v = Tu$  represent electron and hole excitations, respectively. The Hamiltonian  $\hat{h}_K$  and  $\hat{h}_{K'}$  in the vicinity of  $K$  and  $K'$  points can be derived based on the nearest-neighbor tight-binding model with the  $\mathbf{k} \cdot \mathbf{p}$  method or with the effective-mass approximation.<sup>21,22</sup> Near the Dirac cones,  $\hat{h}_K$  and  $\hat{h}_{K'}$  are found as

$$\hat{h}_K = v_F(\sigma_x\pi_x + \sigma_y\pi_y) = v_F \begin{pmatrix} 0 & \pi_x - i\pi_y \\ \pi_x + i\pi_y & 0 \end{pmatrix} \quad (6)$$

and

$$\begin{aligned} \hat{h}_{K'} &= v_F(-\sigma_x\pi_x + \sigma_y\pi_y) \\ &= v_F \begin{pmatrix} 0 & -\pi_x - i\pi_y \\ -\pi_x + i\pi_y & 0 \end{pmatrix}, \end{aligned} \quad (7)$$

where  $\pi = \mathbf{p} + e\mathbf{A}$  and  $v_F = v_F^G\Theta(-x) + v_F^S\Theta(x)$ ,  $v_F^D$  and  $v_F^S$  are the Fermi velocities in the graphene and superconductor. The time reversal operator in Eq. (1) takes the form  $T = \begin{pmatrix} 0 & I_{2 \times 2} \\ I_{2 \times 2} & 0 \end{pmatrix} \mathcal{C} = T^{-1}$  with  $\mathcal{C}$  the operator of complex conjugation. According to the Hamiltonian, the wave function can be written as,

$$\Psi = (\psi_{AK}^{(e)}, \psi_{BK}^{(e)}, \psi_{AK'}^{(e)}, \psi_{BK'}^{(e)}, \psi_{AK}^{(h)}, \psi_{BK}^{(h)}, \psi_{AK'}^{(h)}, \psi_{BK'}^{(h)})^T,$$

where  $T$  stands for transpose. Because both inequivalent sublattices are on the interface for the armchair configuration, the interface potential is presented by delta potentials  $V_{AK}(\mathbf{r}) = V_0\delta(x=0)$ ,  $V_{BK}(\mathbf{r}) = V_0\delta(x=0)$ ,  $V_{AK'}(\mathbf{r}) = V_0\delta(x=0)$ , and  $V_{BK'}(\mathbf{r}) = V_0\delta(x=0)$  for the atoms at A and B sublattices. Employing the wavefunctions given in Eqs. (4) and (5), the interface potential in the basis  $\psi_{A/B,K/K'}^{(e)}$ ,  $\psi_{A/B,K/K'}^{(h)}$  is given as

$$\hat{V} = V_0 \begin{pmatrix} I_{2 \times 2} & I_{2 \times 2} \\ I_{2 \times 2} & I_{2 \times 2} \end{pmatrix}. \quad (8)$$

For convenient calculations, we introduce an unitary transformation,

$$\Lambda = \begin{pmatrix} \Pi_{4 \times 4} & 0 \\ 0 & \Pi_{4 \times 4} \end{pmatrix} \quad (9)$$

with

$$\Pi_{4 \times 4} = \begin{pmatrix} I_{2 \times 2} & 0 \\ 0 & \sigma_z \end{pmatrix}. \quad (10)$$

Under this unitary transformation, the Hamiltonian in Eq. (1) becomes,

$$\hat{\mathcal{H}}' = \Lambda \hat{\mathcal{H}} \Lambda^\dagger = \begin{pmatrix} \hat{h}' - E_F & \Delta \cdot I_4 \\ \Delta^* \cdot I_4 & E_F - T'\hat{h}'T'^{-1} \end{pmatrix}, \quad (11)$$

where

$$\hat{h}' = \begin{pmatrix} \hat{h}'_K & 0 \\ 0 & \hat{h}'_{K'} \end{pmatrix} + U(x) + \hat{V}'(x) \quad (12)$$

and

$$\hat{V}' = \Pi_{4 \times 4} \hat{V} \Pi_{4 \times 4}^\dagger = V_0 \begin{pmatrix} I_{2 \times 2} & \sigma_z \\ \sigma_z & I_{2 \times 2} \end{pmatrix} \quad (13)$$

with

$$\hat{h}'_K = v_F(\sigma_x\pi_x + \sigma_y\pi_y), \quad (14)$$

$$\hat{h}'_{K'} = v_F(\sigma_x\pi_x - \sigma_y\pi_y). \quad (15)$$

Here we notice that  $T'\hat{V}'T'^{-1} = \hat{V}'$ . Correspondingly, the wavefunction is given by  $\hat{\Psi} = \Pi_{4 \times 4}\Psi$ , i.e.,

$$\tilde{\Psi} = (\psi_{AK}^{(e)}, \psi_{BK}^{(e)}, \psi_{AK'}^{(e)}, -\psi_{BK'}^{(e)}, \psi_{AK'}^{(h)}, \psi_{BK'}^{(h)}, \psi_{AK}^{(h)}, -\psi_{BK}^{(h)})^T.$$

In the spinor representation  $\psi = (u, v)^T$ , it corresponds to a transformed form

$$\tilde{\Psi} = (\tilde{u}_{AK}, \tilde{u}_{BK}, \tilde{u}_{AK'}, \tilde{u}_{BK'}, \tilde{v}_{AK'}, \tilde{v}_{BK'}, \tilde{v}_{AK}, \tilde{v}_{BK})^T.$$

To obtain the boundary conditions for the electron and hole excitations, we integrate DBdG equation cross over the interface. Due to the features of a delta-type of interface potential and first order differential equation of DBdG, the wavefunctions are discontinuous crossing the interface between the graphene and superconductor. Consequently, the particle-like and hole-like components require to satisfy following boundary conditions

$$\begin{aligned} \tilde{u}_{AK}(0^+) + \tilde{u}_{AK'}(0^+) &= \tilde{u}_{AK}(0^-) + \tilde{u}_{AK'}(0^-), \\ \tilde{v}_{AK}(0^+) + \tilde{v}_{AK'}(0^+) &= \tilde{v}_{AK}(0^-) + \tilde{v}_{AK'}(0^-), \\ \tilde{u}_{BK}(0^+) - \tilde{u}_{BK'}(0^+) &= \tilde{u}_{BK}(0^-) - \tilde{u}_{BK'}(0^-), \\ \tilde{v}_{BK}(0^+) - \tilde{v}_{BK'}(0^+) &= \tilde{v}_{BK}(0^-) - \tilde{v}_{BK'}(0^-), \\ \tilde{u}_{AK}(0^+) - \tilde{u}_{AK}(0^-) &= -i\tilde{V}_0[\tilde{u}_{BK}(0) - \tilde{u}_{BK'}(0)], \\ \tilde{v}_{AK'}(0^+) - \tilde{v}_{AK'}(0^-) &= -i\tilde{V}_0[-\tilde{v}_{BK}(0) + \tilde{v}_{BK'}(0)], \\ \tilde{u}_{BK}(0^+) - \tilde{u}_{BK}(0^-) &= -i\tilde{V}_0[\tilde{u}_{AK}(0) + \tilde{u}_{AK'}(0)], \\ \tilde{v}_{BK'}(0^+) - \tilde{v}_{BK'}(0^-) &= -i\tilde{V}_0[\tilde{v}_{AK}(0) + \tilde{v}_{AK'}(0)], \end{aligned} \quad (16)$$

where  $\tilde{V}_0 = V_0/2\hbar((v_F^G)^{-1} + (v_F^S)^{-1})$ . This implies that the boundary conditions manifest a linear combination of states from two valleys in the armchair configuration. This stems from that fact that both inequivalent sublattices appear at the interface. For simplify, we will omit the wavy line above the wavefunction from now on.

### 3. Energy Spectra and Effective Charges

#### 3.1 Wavefunctions in the graphene and superconductor regions

The eigenstates in graphene and superconductor can be obtained by solving the DBdG equations in these two regions separately. We assume that the excitation gap is real and isotropic,  $\Delta(\mathbf{r}) = \Delta_0\theta(x)$ , in both the sublattice and the valley degrees of freedom. In addition, the energies of charge carriers in graphene is restricted in a window  $|E| \leq \Delta_0$ , so that electron and hole excitations with  $|E| \leq \Delta_0$  are confined on the graphene side in a width of a magnetic length  $l_B$  in the vicinity of interface by the magnetic field. For a magnetic field perpendicular to the graphene sheet,  $\mathbf{B} = (0, 0, B)$ , the vector potential is given as  $\mathbf{A} = (0, Bx, 0)\Theta(-x)$ .

The eigenvalues of the DBdG equation in the region of a graphene ( $x < 0$ ) are found as  $E_{n,\gamma\delta} = \gamma\delta\sqrt{2n} + (-1)^\delta E_F$ , where  $n$  is any positive integer,  $\delta = 1, 2$  indicate the electrons and holes, respectively, and  $\gamma\delta = \pm 1$  represent the solutions for the conduction band and the valence band. Based on the eigenstates the wavefunction for the energy  $E$  (i.e.,  $z$ ) and the wavevector  $k_y$  in the graphene side can be written as

$$\Psi_{\kappa,\eta}^{G\lambda}(x, y, k_y, z_\eta) = \frac{1}{\sqrt{L_y}} e^{ik_y y} \Phi_{\kappa,\eta}^{G\lambda}(x, k_y, z_\eta) \quad (17)$$

with

$$\begin{aligned} \Phi_{+,+}^{G\lambda}(x, k_y, z_+) &= (i\sqrt{z_+} D_{z_+ - 1}(\lambda\sqrt{2}(x + k_y)), D_{z_+}(\lambda\sqrt{2}(x + k_y)), 0, 0, 0, 0, 0, 0)^T, \\ \Phi_{-,+}^{G\lambda}(x, k_y, z_+) &= (0, 0, D_{z_+}(\lambda\sqrt{2}(x + k_y)), i\sqrt{z_+} D_{z_+ - 1}(\lambda\sqrt{2}(x + k_y)), 0, 0, 0, 0)^T, \\ \Phi_{+,-}^{G\lambda}(x, k_y, z_-) &= (0, 0, 0, 0, D_{z_-}(\lambda\sqrt{2}(x - k_y)), -i\sqrt{z_-} D_{z_- - 1}(\lambda\sqrt{2}(x - k_y)), 0, 0)^T, \\ \Phi_{-,-}^{G\lambda}(x, k_y, z_-) &= (0, 0, 0, 0, 0, 0, -i\sqrt{z_-} D_{z_- - 1}(\lambda\sqrt{2}(x - k_y)), D_{z_-}(\lambda\sqrt{2}(x - k_y)))^T, \end{aligned} \quad (18)$$

where  $z_\eta = (E + \eta E_F)^2/2$  is parameter to be obtained self-consistently from the boundary conditions, and  $D_z(x)$  is a parabolic cylinder function.  $\lambda = \pm 1$  for the pseudospin A (+) and B (-) subspaces,  $\kappa = \pm 1$  for the  $K$  (+) and  $K'$  (-) valleys, and  $\eta = \pm 1$  for electrons (+) and holes (-), respectively. Here, we use the unit where the length is scaled by  $l_B$  and the energy is scaled by  $E_0 = \hbar v_F^G/l_B$ , respectively. We also define the guiding-center coordinates  $X_{k_y} = -k_y l_B^2$  and  $-X_{k_y}$  for the cyclotron motion of electrons and holes in the normal region.

In the same way, the eigenvalues of the DBdG equation in the superconductor side are found as  $E_{\alpha\beta} = \alpha\sqrt{[U_0 + E_F + \beta(v_F^S/v_F^G)k]^2 + \Delta_0^2}$ , where  $\alpha = \pm 1$  for the electron and hole bands, respectively,  $\beta = \pm 1$  and  $k = \sqrt{k_x^2 + k_y^2}$ . The wavefunction for the energy  $E$  and the wavevector  $k_y$  in the superconductor side can be written as,

$$\Psi_{\kappa,\eta}^{S\lambda}(x, y, k_y, E) = \frac{1}{\sqrt{L_y}} e^{\lambda i k_x^{(\eta)} x + i k_y y} \Phi_{\kappa,\eta}^{S\lambda}(k_y, E), \quad (19)$$

with

$$\begin{aligned} \Phi_{+,\eta}^{S\lambda}(k_y, E) &= \left( \exp\left(i\frac{\phi + \eta\theta}{2}\right) \frac{\lambda k_x^{(\eta)} - i k_y}{k_\eta} \exp\left(i\frac{\phi + \eta\theta}{2}\right), 0, 0, \exp\left(-i\frac{\phi + \eta\theta}{2}\right) \frac{\lambda k_x^{(\eta)} - i k_y}{k_\eta}, \exp\left(-i\frac{\phi + \eta\theta}{2}\right), 0, 0 \right)^T, \\ \Phi_{-,\eta}^{S\lambda}(k_y, E) &= \left( 0, 0, \exp\left(i\frac{\phi + \eta\theta}{2}\right) \frac{\lambda k_x^{(\eta)} + i k_y}{k_\eta} \exp\left(i\frac{\phi + \eta\theta}{2}\right), 0, 0, \exp\left(-i\frac{\phi + \eta\theta}{2}\right) \frac{\lambda k_x^{(\eta)} + i k_y}{k_\eta}, \exp\left(-i\frac{\phi + \eta\theta}{2}\right) \right)^T, \end{aligned} \quad (20)$$

where the meaning of  $\kappa$  and  $\lambda$  are defined as those for the graphene,  $\theta = \tan^{-1} \sqrt{(\Delta_0/E)^2 - 1}$ ,  $k_x^{(\eta)} = \eta k' + i k''$  with  $k' = \text{sign}[U_0 + E_F](v_F^G/v_F^S)\sqrt{[(U_0 + E_F)(\Xi + \Gamma)]}$ ,  $k'' = (v_F^G/v_F^S)\sqrt{[(U_0 + E_F)(\Gamma - \Xi)]}$ ,  $\Xi = [(U_0 + E_F)^2 - \Delta_0^2 + E^2 - (v_F^S/v_F^G)^2 k_y^2]/[2|U_0 + E_F|]$ , and  $\Gamma = \sqrt{\Delta_0^2 - E^2 + \Xi^2}$ .

Using  $\Psi_{\kappa,\eta}^{G\lambda}(x, y, k_y, E)$  and  $\Psi_{\kappa,\eta}^{S\lambda}(x, y, k_y, E)$ , the wavefunctions in the graphene and superconductor regions can then be expressed in the form  $\Psi^N(x, y, k_y, E) = \sum_{\kappa,\eta,\lambda} c_{\kappa,\eta}^\lambda \Psi_{\kappa,\eta}^{G\lambda}(x, y, k_y, E)$  and  $\Psi^S(x, y, k_y, E) = \sum_{\kappa,\eta,\lambda} d_{\kappa,\eta}^\lambda \Psi_{\kappa,\eta}^{S\lambda}(x, y, k_y, E)$ , respectively. The coefficients  $c_{\kappa,\eta}^\lambda$  and  $d_{\kappa,\eta}^\lambda$  can be determined by the boundary conditions. For  $\Psi_{\kappa,\eta}^{G\lambda}$  those with  $\lambda = +1$  are divergent when  $x \rightarrow -\infty$ , so  $c_{\kappa,\eta}^+ = 0$ . Similarly,  $d_{\kappa,\eta}^- = 0$ . In general, the boundary conditions yield an homogeneous linearity equation of  $c_{\kappa,\eta}^\lambda$  and  $d_{\kappa,\eta}^\lambda$ . We can find the energy spectrum from the condition for existing nonzero solution. The remaining coefficient (for example  $c_{\kappa,+}^-$ ) can be decided by the normalization condition  $\int_{-\infty}^{+\infty} \int_{L_y} dx \Psi^\dagger(x, y) \Psi(x, y) = 1$ , i.e.,

$$\begin{aligned}
 1 = & \sum_{\kappa=\pm, \eta=\pm} |c_{\kappa,\eta}^-|^2 \int_{-\infty}^0 dx \{D_{z\eta}^2(-\sqrt{2}(x + \eta k_y)) \\
 & + z_\eta D_{z\eta-1}^2(-\sqrt{2}(x + \eta k_y))\} \\
 & + \sum_{\kappa=\pm} (|d_{\kappa,+}^+|^2 + |d_{\kappa,-}^+|^2) \frac{1}{k''} \left( \left| \frac{k_x^+ - \kappa i k_y}{k_+} \right|^2 + 1 \right) \\
 & + 2 \sum_{\kappa=\pm} \text{Re} \left\{ i d_{\kappa,+}^{+*} d_{\kappa,-}^+ \frac{E}{\Delta_0 k_x^-} \right. \\
 & \left. \times \left[ \left( \frac{k_x^+ - i k k_y}{k_+} \right)^* \frac{k_x^- - i k k_y}{k_-} + 1 \right] \right\}. \quad (21)
 \end{aligned}$$

After performing these procedures, we can obtain the energy spectrum and wavefunctions for whole region.

### 3.2 $X_{k_y}$ -dependence of energy spectrum $E_N(X_{k_y})$

By including a delta-function potential of strength  $V_0$  at the interface, the contact of graphene and superconductor can be regarded as a metallic contact for  $V_0 = 0$  and a tunneling junction for a finite value of  $V_0$ . The  $X_{k_y}$ -dependence of  $E_N(X_{k_y})$  manifests the existence of edge states. The dispersion of edge states is sensitive to both the Fermi energy  $E_F$  and the strength of the interface potential  $V_0$ .

In this work our purpose is to demonstrate that for a strongly coupled G/S system, charge neutral Fermionic states can exist in all LLs. The necessary conditions for strong G/S coupling and charge neutral states in high LLs are a near zero Fermi energy and a small superconductor pair potential. For typical s-wave superconductors, the pair potential is very small  $\Delta_0/E_0 \sim 1$ . There is a significant difference between the energy spectra for large  $\Delta_0$  and small  $\Delta_0$ . We first examine the spectra with a large (unrealistic)  $\Delta_0/E_0 \gg 1$ . This situation was previously studied in Ref. 13. The inset of Fig. 2 shows the energy spectra for  $\Delta_0/E_0 = 10$  under two different interface potentials,  $V_0 = 0$  and  $V_0 = 10000$  (all energies are in unit of  $E_0$ ). For  $V_0 = 0$ , there is a valley degeneracy. The left side is for the electron-like particles while right side is for the hole-like particles. For non-zero interface potential  $V_0 = 10000$  the valley degenerate is lifted and energy levels are split in the region of the intermediate values of  $X_{k_y}$ . In general, the splitting enlarges as the  $V_0$  increases. The AR induced mixing between electron- and hole-like levels becomes weaker with  $V_0$  increasing, or the normal reflection turns to stronger. For larger  $|X_{k_y}|$  these levels trend to the same asymptotic degenerate levels. So the delta potential strength  $V_0$  could tune the proportion of the

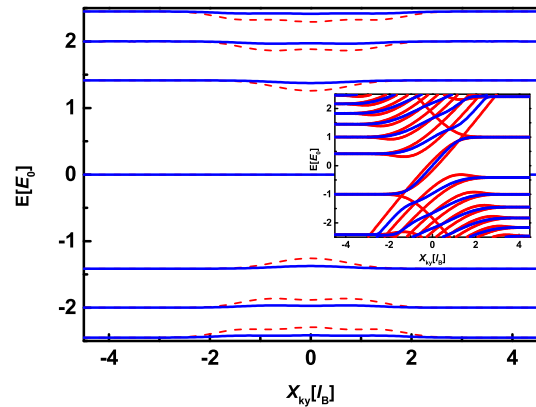


**Fig. 2.** (Color online) The energy dispersion for  $E_F = 0$ , the red dash line is for the pair potential  $\Delta_0 = 2.5$  and the blue line is for  $\Delta_0 = 10$ . Inset: Energy dispersion relation  $E_N(X_{k_y})$  for Fermi energy  $E_F = 1$  and the pair potential  $\Delta_0 = 10$ . The blue line is for  $V_0 = 0$ . The red lines represent the K and K' valleys, respectively, for  $V_0 = 10000$ .

AR at the boundary. The  $X_{k_y}$ -dependent energy spectrum has the symmetry  $E_N(X_{k_y}) = -E_{-N}(-X_{k_y})$ .

The interplay of cyclotron motion in the graphene region and the AR from the interface with the superconductor region results in the formation of chiral Dirac–Andreev edge states with guiding-center-dependent electric charge<sup>19</sup> for  $|E| < \Delta_0$ . These solutions can be described as interface states in the sense that they are localized electron states in the direction perpendicular to the interface and propagate along the interfaces, in analogy to the edge states of a semi-infinite graphene in a magnetic field. In contrast with conventional edge states, the  $V_0 = 0$  interface does not cause splitting of the dispersion. This is a consequence that at the G/S interface with  $V_0 = 0$ , the wave function is finite and continuous and the associated probability density can be finite in the superconductor region.

We found that for a small (more realistic)  $\Delta$  and  $E_F = 0$  (for AR to dominate) G/S coupling becomes very strong and qualitatively alters the energy dispersion. Figure 2 shows the clear and convincing evidence of the G/S coupling of the hybrid. For  $E_F = 0$  the reflection is in the SAR regime. For a large superconductor pair potential, the G/S coupling is very weak. Therefore the energy levels are approximately the Landau levels of graphene. This is shown with blue curves. For a small superconductor pair potential, the coupling of the graphene with the superconductor results in a decrease of the energy levels. The coupling is stronger where the carrier density is higher in the graphene. Since the density of a Landau level varies with  $X_{k_y}$ , the energy becomes dispersive with  $X_{k_y}$ . For  $N = 1$ , the carrier concentration peaks at  $X_{k_y} = 0$  and thus the energy minimum occurs at  $X_{k_y} = 0$ . For  $N = 2$  the carrier concentration has two peaks at finite  $X_{k_y}$  and the energy dispersion has two minima at finite  $X_{k_y}$ . For the  $N$ th Landau level, there are  $N$  concentration maxima. The number of energy minima equals the number of concentration maxima.

### 3.3 Effective electrical charge of the single-particle excitations

As in the case for Bogoliubov quasiparticles in a conventional superconductor, the Dirac–Andreev edge states

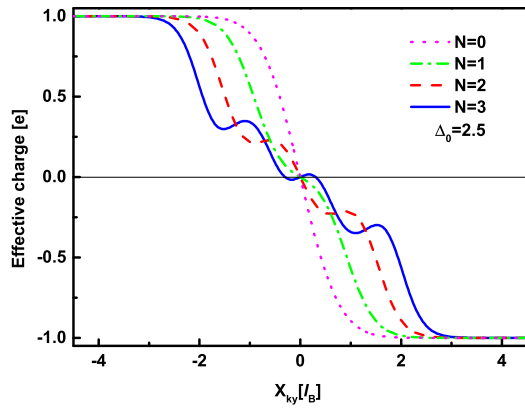


**Fig. 3.** (Color online) Effective electric charge  $e^{(N, X_{ky})}$  of the single-particle excitations as a function of  $X_{ky}$  (in units of  $l_B$ ) for  $N = 0, 1, 2, 3$  Landau branches as shown in the legend. The delta potential strength is  $V_0 = 0$  and  $\Delta_0 = 2.5$ .

are coherent superpositions of particles and holes. Consequently, their effective electrical charge generally has a nonquantized value and is given by

$$e^{(\Psi)} = \int d^2r [\Psi(r)]^\dagger \Sigma_z \Psi(r), \quad (22)$$

where  $\Sigma_z = \begin{pmatrix} I_4 & 0 \\ 0 & -I_4 \end{pmatrix}$ .

The calculated effective charges  $e^{(N, X_{ky})}$  of states  $\Psi_N(X_{ky})$  for  $N = 0, 1, 2, 3$  with  $V_0 = 0$  are shown in Fig. 3 as a function of  $X_{ky}$ . The effective charge changes the sign, which indicates the presence of a neutral Fermionic mode at a finite value of  $X_{ky}$ . The neutral Fermionic mode has been demonstrated recently in a TI/S hybrid.<sup>19)</sup> The mechanism and properties of the neutral Fermionic states presented here for the G/S hybrid are quite different to that in a TI/S hybrid. The neutral Fermionic state in a G/S hybrid is due to the coupling between orbital motion and the pseudo spin. The mathematical structure of the Hamiltonian is very similar for both systems. For  $N = 0$  mode,  $e^{(0, -X_{ky})} = -e^{(0, X_{ky})}$ . The  $N = 0$  state has zero effective charge at  $X_{ky} = 0$ . The more remarkable picture here is that, for a zero Fermi level, the neutral Fermionic state can also exist in higher Landau levels, i.e.,  $e^{(-N, -X_{ky})} = -e^{(N, X_{ky})}$ . This results in a zero effective charge at  $X_{ky} = 0$  for  $N \neq 0$ . This effect is totally missing in a TI/S hybrid. The result is a direct consequence of DBdG equation. As mentioned early the definition of the effective charge given by Eq. (5) is not a quantum number and it is possible for it to acquire any value. For the  $N = 0$  LL, the

$$\begin{aligned} \Psi &= (u_{AK}, u_{BK}, u_{AK'}, u_{BK'}, v_{AK'}, v_{BK'}, v_{AK}, v_{BK})^T \\ &= (u_K, u_{K'}, v_{K'}, v_K)^T = (u, v)^T, \end{aligned} \quad (24)$$

the following continuity equation for the probability current

$$\partial_t \begin{pmatrix} \rho^u \\ \rho^v \end{pmatrix} + \partial_y \begin{pmatrix} J^u \\ J^v \end{pmatrix} = \begin{pmatrix} S \\ -S \end{pmatrix} \quad (25)$$

are got, where

$$S = \frac{2\text{Im}(\Delta u^\dagger v)}{\hbar}. \quad (26)$$

Specific to the NS graphene junction described in this paper, the current flows in  $y$ -direction. So, we look at the currents

charge neutral state has a unique property that its antiparticle is itself. For the charge neutral states in high LLs, this requirement is not satisfied. In the present system, the symmetry  $e^{(N, -X_{ky})} = -e^{(N, X_{ky})}$  is maintained but clearly the antiparticle of the charge neutral state in the  $N$ th LL is not itself. We note that the effective charge in the high LL can also acquire a zero value in a TI/S hybrid.<sup>19)</sup> However, in the TI/G hybrid it occurs at finite wavenumbers and does not have the symmetry of  $e^{(N, -X_{ky})} = -e^{(N, X_{ky})}$ . This symmetry in the G/S hybrid is a direct consequence of valley degeneracy in the graphene and the Andreev reflection at the interface. Formation of charge neutral states is of importance in understanding the nature of the interface states in a G/S hybrid. At the G/S interface, an incident electron in the K-valley can only pair with another electron in the K'-valley.

Although the charge neutral Fermionic states reported here have the property of  $e^{(N, 0)} = 0$ , they are not strictly Majorana mode. Such non-Majorana charge neutral modes can result in interesting physical properties. For example, a totally different type of charge neutral Fermionic modes have been proposed and detected in fractional quantum Hall states.<sup>23,24)</sup> These modes played an important role in understanding the fractional quantum Hall states of  $\nu = 8/3, 7/3$ . Recently chiral edge states with neutral fermions has been observed in synthetic Hall ribbons.<sup>18)</sup>

A solution of electronic state being electrically neutral is not only important conceptually in understanding why they behave as they do, it is also useful in the quantitative analysis, because it provides a link between the concentrations of the incident electrons and the reflected holes. A most important consequence of this principle is that it is not possible to add a single species of electron to a solution all by itself. Some other species of opposite charge (reflection hole) must always be added at the same time, and its amount and identity must be incorporated into calculations of effective charge.

## 4. Edge Current in the Vicinity of G/S Interface

### 4.1 Formulation of charge current density

The edge states can produce the current in the vicinity of both sides of interface. Starting from the time-dependent version of the DBdG Eq. (1)

$$i\hbar \frac{\partial}{\partial t} \Psi = \widehat{\mathcal{H}} \Psi \quad (23)$$

with the wave function:

near the interface where for each quasiparticle state  $M = [X_{ky}, E(X_{ky})]$  in the spectrum the electron-like and hole-like excitations probability currents density<sup>25)</sup>  $J_M^u$  and  $J_M^v$  are

$$J_M^u = v_F [u_K^\dagger \sigma_y u_K - u_{K'}^\dagger \sigma_y u_{K'}] \quad (27)$$

and

$$J_M^v = -v_F [v_K^\dagger \sigma_y v_K - v_{K'}^\dagger \sigma_y v_{K'}]. \quad (28)$$

Sum over all quasiparticle states and the charge current density at the interface is found as

$$\begin{aligned}
 J &= e \sum_M (f_M J_M^u + (1 - f_M) J_M^v) \\
 &= e v_F \sum_M (f_M (u_K^\dagger \sigma_y u_K - u_{K'}^\dagger \sigma_y u_{K'}) \\
 &\quad - (1 - f_M) (v_K^\dagger \sigma_y v_K - v_{K'}^\dagger \sigma_y v_{K'})) \\
 &= e v_F \sum_M (f_M (u_K^\dagger \sigma_y u_K - u_{K'}^\dagger \sigma_y u_{K'} + v_K^\dagger \sigma_y v_K - v_{K'}^\dagger \sigma_y v_{K'}) \\
 &\quad - (v_K^\dagger \sigma_y v_K - v_{K'}^\dagger \sigma_y v_{K'})), \quad (29)
 \end{aligned}$$

where  $f_M = f_0(E - \gamma E_F)$ ,  $f_0(E) = \frac{1}{e^{\beta E} + 1}$  is the Fermi–Dirac distribution,  $E_F$  is the Fermi energy at the superconductivity region, and  $\gamma = 1$  ( $-1$ ) for the electron (hole) component. The formulation for the current of BdG equation is defined in Ref. 26 by written in terms of a sum over quasiparticle states,  $J = J_{BdG} + J_{VAC}$  where the BdG quasiparticle component of the electron current is given by the term linear in  $\{f_M\}$  and on the other hand, the condensate vacuum current is identified with the term which is independent of the occupation probabilities  $\{f_M\}$ , i.e.,

$$J_{BdG} = e \sum_M [J_M^u - J_M^v] f_M \quad (30)$$

and

$$J_{VAC} = e \sum_M J_M^v. \quad (31)$$

All the states below the Fermi energy can contribute to the current. Taking account all the states, the spatial distributions of charge currents can written in the form

$$\begin{aligned}
 J^L &= \int dk_y \sum_{E(X_{k_y})} \left[ f_F(E) (|c_{++}^-|^2 + |c_{--}^-|^2) \frac{(E + E_F)}{\sqrt{2}} \right. \\
 &\quad \times D_{z_+ - 1}(-\sqrt{2}(x + k_y)) D_{z_+}(-\sqrt{2}(x + k_y)) \\
 &\quad - (1 - f_F(E)) (|c_{+-}^-|^2 + |c_{-+}^-|^2) (E - E_F) / \sqrt{2} D_{z_+ - 1} \\
 &\quad \left. \times (-\sqrt{2}(x - k_y)) D_{z_+}(-\sqrt{2}(x - k_y)) \right] \quad (32)
 \end{aligned}$$

in the graphene region and

$$\begin{aligned}
 J^R &= \frac{v_F^S}{v_F^G} \sum_{E(k_y)} \int dk_x e^{-2k'_x} 2 \sum_{\kappa=\pm} \kappa \left\{ (f_F(E) - 1) (|d_{\kappa+}^+|^2 \right. \\
 &\quad + |d_{\kappa-}^+|^2) \text{Im} \left( \frac{k_x^{(+)} - ik_k y}{k_+} \right) \\
 &\quad + f_F(E) 2 \cos \theta \text{Im} \left[ d_{\kappa+}^+ d_{\kappa-}^{+*} e^{2ik'_x} \frac{(k_x^{(+)} - ik_k y)}{k_+} \right] \\
 &\quad \left. - 2 \text{Im} \left[ d_{\kappa+}^+ d_{\kappa-}^{+*} e^{2ik'_x} e^{-i\theta} \frac{(k_x^{(+)} - ik_k y)}{k_+} \right] \right\} \quad (33)
 \end{aligned}$$

in the superconductor region.

#### 4.2 Distribution of equilibrium edge current

Because we are interested in those contributions due to the AR, only those states in the gap window of the superconductor,  $|E| \leq \Delta_0$ , are considered in the calculations of current. The distribution of equilibrium edge current at zero temperature for zero and finite interface potential barrier  $V_0$  is shown in Figs. 4 and 5. We take the value of magnetic field used in experiment  $B = 3.7$  T.<sup>27–29</sup> Correspondingly,  $E_0 = \hbar v_F^G / l_B = 50$  meV.

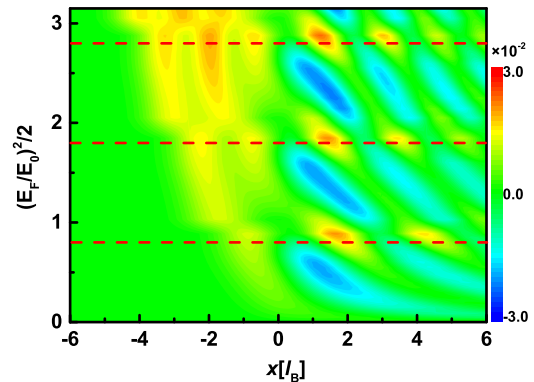


**Fig. 4.** (Color online) The energy-dependent current density (in unit of  $\frac{e^2 B v_F}{\pi \hbar}$ ) in the region near armchair boundary.  $B = 3.7$  T,  $\Delta_0 = 1.0$  meV, and  $V_0 = 0$ .

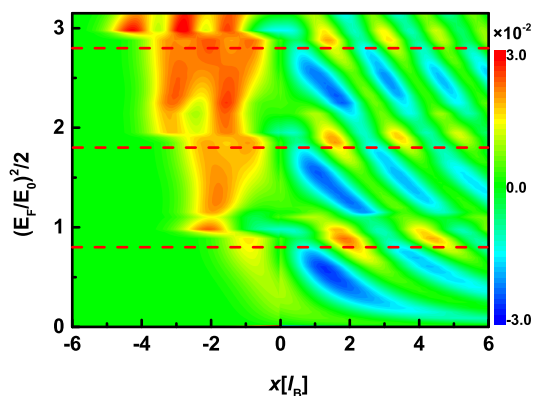


**Fig. 5.** (Color online) The energy-dependent current density (in unit of  $\frac{e^2 B v_F}{\pi \hbar}$ ) in the region near armchair boundary.  $B = 3.7$  T,  $\Delta_0 = 1.0$  meV, and  $V_0 = 25$  meV  $l_B$ .

As shown in Figs. 4 and 5, in the graphene region far away from the boundary, the current density is zero due to the wave function of one state with given  $k_y$  is antisymmetric relative to the point  $X_{k_y}$ . This is consistent with that the states localized deep inside the system are not influenced by the boundary. For the edge states, due to the reflection at the boundary, the current density becomes nonzero. In the superconductor region, the phase information of quasiparticle excitations is preserved during their traversal in the G/S hybrid and gives rise to quantum interference effects in the spatial current density. Therefore, the current density is oscillatory and the amplitude decays away from the interface in the superconductor region.

The distribution of current density depends on the occupation of Landau levels. Each time when the Fermi level crosses a Landau level, there is an additional contribution to the current. In the graphene region it is found that the higher the Fermi level is, the wider region the state occupies and the more channels contribute to the current density, shown in Figs. 4 and 5. It should be noted that in the calculation of the current spatial distribution of half-infinite graphene, all states below the Fermi energy are included. Now the states included not only need to be below the Fermi energy but also should be restricted within the superconductor energy gap. Carriers with energy greater than the gap contribute to the normal current which does not depend on the G/S coupling. In the specific

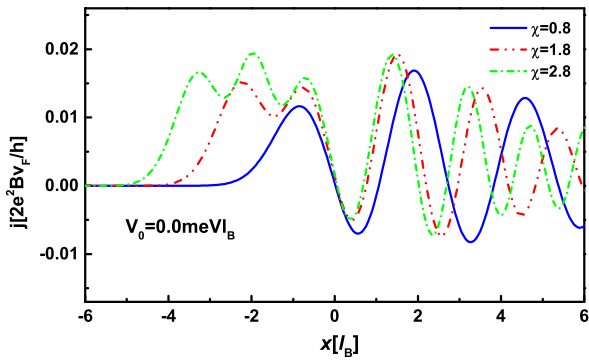


**Fig. 6.** (Color online) The energy-dependent current density in the region near armchair boundary at the selected Fermi energies, where  $\chi = (E_F/E_0)^2/2$ ,  $\Delta_0 = 1.0$  meV, and  $V_0 = 0$ .

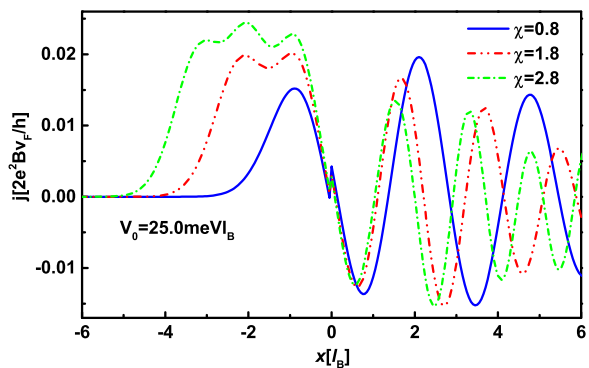


**Fig. 7.** (Color online) The energy-dependent current density in the region near armchair boundary at the selected Fermi energies, where  $\chi = (E_F/E_0)^2/2$ ,  $\Delta_0 = 1.0$  meV, and  $V_0 = 25$  meV  $l_B$ .

situation in which the superconductor energy gap is the same as the Fermi energy and in the infinite potential limit, we can recover the current distribution in Ref. 9. In the superconductor region, the current density at the boundary oscillates with the filling factor as shown in Figs. 6 and 7. But with the filling factor increasing, the oscillatory frequency at a fixed position in a period becomes smaller with more Landau levels. The oscillatory frequency decreases gradually though their initial phases at the boundary as  $\chi = (E_F/E_0)^2/2$  increases from 0.8 to 2.8.

The effect of neutral Fermionic states on the current distribution can be seen from the position dependent current density. As expected, at high energy (or large  $\chi$ ) more levels will contribute to the current in the graphene side. (i) In comparison of Figs. 6 and 7, it is found that the current characteristics that is unique to the present system is the current discontinuity at the boundary in the presence of nonzero interface potential. This discontinuity of current density arises from the discontinuity in the wave functions crossing the boundary where the interface potential is nonzero. Since the current operator is proportional to the wave functions, a current density discontinuity appears at the interface. The current density at the interface becomes continuous for a perfect interface, as shown in Fig. 6. (ii) At the interface the current density is zero indicating missing charges of quasi-particles at the interface. This is a direct consequence that effective charge for all Landau levels are zero at the interface, as shown in Fig. 3. We propose that the

missing current has the origin of formation of charge neutral Fermionic states near the boundary. These neutral states do not contribute to the current in the vicinity of the boundary. It can be shown that for graphene/metal junctions, there is no zero current density at the interface.

## 5. Concluding Remarks

In conclusion, we have demonstrated the interface electronic properties due to the normal state/superconductor coupling in a G/S hybrid. The coupling gives rise to the formation of charge neutral Fermionic states in the ground state and in all excited states. Because the zero effective charges in all states at the interface, the electrical current density vanished at the interface. In the absence of an interface potential the current density is continuous crossing the interface. In the case of a finite interface potential, a current density discontinuity appears at the interface.

## Acknowledgments

The authors are thankful for the support of NSFC (11274013), NBRP of China (2012CB921300), and the Australian Research Council (DP160101474).

- 1) C. W. J. Beenakker, *Phys. Rev. Lett.* **97**, 067007 (2006).
- 2) K. Komatsu, C. Li, S. Autier-Laurent, H. Bouchiat, and S. Guéon, *Phys. Rev. B* **86**, 115412 (2012).
- 3) A. F. Andreev, *Sov. Phys. JETP* **19**, 1228 (1964).
- 4) A. F. Andreev, *Sov. Phys. JETP* **22**, 455 (1966).
- 5) J. Linder and A. Sudbø, *Phys. Rev. Lett.* **99**, 147001 (2007).
- 6) J. Linder and A. Sudbø, *Phys. Rev. B* **77**, 064507 (2008).
- 7) S. Bhattacharjee and K. Sengupta, *Phys. Rev. Lett.* **97**, 217001 (2006).
- 8) S. Bhattacharjee, M. Maiti, and K. Sengupta, *Phys. Rev. B* **76**, 184514 (2007).
- 9) W. Wang and Z. S. Ma, *Eur. Phys. J. B* **81**, 431 (2011).
- 10) J. Nitta, T. Akazaki, and H. Takayanagi, *Phys. Rev. B* **49**, 3659 (1994).
- 11) J. P. Heida, B. J. van Wees, T. M. Klapwijk, and G. Borghs, *Phys. Rev. B* **57**, R5618 (1998).
- 12) G. H. Li and E. Y. Andrei, *Nat. Phys.* **3**, 623 (2007).
- 13) A. R. Akhmerov and C. W. J. Beenakker, *Phys. Rev. Lett.* **98**, 157003 (2007).
- 14) C. W. J. Beenakker, *Rev. Mod. Phys.* **80**, 1337 (2008).
- 15) J. Tworzydło, I. Synman, A. R. Akhmerov, and C. W. J. Beenakker, *Phys. Rev. B* **76**, 035411 (2007).
- 16) L. Fu and C. L. Kane, *Phys. Rev. Lett.* **102**, 216403 (2009).
- 17) D. J. Clarke, J. Alicea, and K. Shtengel, *Nat. Phys.* **10**, 877 (2014).
- 18) M. Mancini et al., *arXiv:1502.02495v1*.
- 19) R. P. Tiwari, U. Zülicke, and C. Bruder, *Phys. Rev. Lett.* **110**, 186805 (2013).
- 20) P. G. de Gennes, *Superconductivity of Metals and Alloys*, Addison-Wesley, Reading, MA, 1989.
- 21) T. Ando, *J. Phys. Soc. Jpn.* **74**, 777 (2005).
- 22) M. Koshino, T. Nakanishi, and T. Ando, *Phys. Rev. B* **82**, 205436 (2010).
- 23) M. Dolev, Y. Gross, R. Sabo, I. Gurman, M. Heiblum, V. Umansky, and D. Mahalu, *Phys. Rev. Lett.* **107**, 036805 (2011).
- 24) N. Read and E. Rezayi, *Phys. Rev. B* **59**, 8084 (1999).
- 25) G. E. Blonder, M. Tinkham, and T. M. Klapwijk, *Phys. Rev. B* **25**, 4515 (1982).
- 26) S. Datta and P. F. Bagwell, *Superlattices Microstruct.* **99**, 051233 (1999).
- 27) P. Rickhaus, M. Weiss, L. Marot, and C. Schönberger, *Nano Lett.* **12**, 1942 (2012).
- 28) E. K. Sichel, H. H. Sample, and J. P. Salerno, *Phys. Rev. B* **32**, 6975 (1985).
- 29) H. Z. Zheng, D. C. Tsui, and A. M. Chang, *Phys. Rev. B* **32**, 5506 (1985).